Materials Research Proceedings 41 (2024) 2702-2709 https://doi.org/10.21741/9781644903131-296

# Study of surface grinding of PEEK parts

SPINA Roberto[1,2,3,a*] and GURRADO Nicola[1,b]

[1]Dip. di Meccanica, Matematica e Management, Politecnico di Bari, Italy

[2]Istituto Nazionale di Fisica Nucleare (INFN) - Sezione di Bari, Italy

[3]Consiglio Nazionale delle Ricerche - Istituto di Fotonica e Nanotecnologie (CNR-IFN), Italy

[a]roberto.spina@poliba.it, [b]nicola.gurrado@poliba.it

**Keywords:** Surface Grinding, PEEK, Statistical Analysis

**Abstract.** The work studies the surface grinding of polyether ether ketone (PEEK) specimens, evaluating material properties and the machining process. An experimental procedure was implemented to collect data during machining to support statistical analysis. Statistical analysis was implemented, mainly based on material properties, which computes roughness achieved after machining by varying cutting speed, feed velocity, and cutting depth, giving helpful information to apply different configurations and strategies.

## Introduction

Precision grinding is one of the primary manufacturing methods for removing materials for finishing surfaces on high-accuracy components, thanks to abrasive grits with different shapes randomly distributed on the grinding wheel. Compared to other machining operations, the material removal mechanism and relative interactions between grits and the workpiece are more complex [1]. The tool consists of randomly oriented, positioned, and shaped grits, acting as cutting edges and individually removing material from the workpiece to produce the final surface. Considering the stochastic nature of the abrasive wheel topography and the high number of process variables, achieving optimum conditions in a repeatable manner based only on experience is very low. Therefore, the process modeling is crucial to design a successful strategy. Once the abrasive wheel topography and grain properties are determined, chip thickness analysis makes force prediction possible. They established force equations for the ploughing and cutting phases, which need experimental calibration. Single grit tests were performed to understand the ploughing mechanism where the measured values are used to calculate the total process forces [2]. Grinding tools are realized in several shapes, sizes, and materials to be adapted to the functional properties of work surfaces for the specific application. The support structure, binder material, and abrasive grits remained the fundamental elements of a grinding tool through the years [3].

Grinding is a significant secondary process applied to parts made with additive manufacturing (AM) to improve the low surface quality resulting at the end of the deposition process. A strict correlation between the process parameters and surface roughness exists, in which the variation of the nozzle and chamber temperatures mainly influenced the roughness values. Poor-quality AM surfaces are obtained with high relative roughness values [4, 5]. Grinding can be combined with AM for improving, repairing, and remanufacturing AM components. This combination allows the full use of individual processes' capabilities while overcoming shortcomings. Because grinding is commonly used at pre- and post-processing stages, improvements are still needed to propose a stable hybrid technology combining additive and subtractive processes in a single system [6]. The non-homogeneous cooling conditions inherent to deposition may vary mechanical properties, leading to a different machining response regarding forces and power consumption, chip morphology, machined surface finish, and integrity. Moreover, residual stresses generated during grinding can lower the performance of the final ground component, with a significant reduction in

fatigue life and the development of subsurface cracking if the grinding process is not accurately controlled [7].

The work aim is to investigate the surface grinding of polyether ether ketone (PEEK) specimens, evaluating material properties and the machining process. The paper initially investigated the setup of the experimental procedure to collect data during grinding. Statistical analysis was then implemented, mainly based on material properties, to compute roughness achieved after grinding by varying cutting speed, feed velocity, and cutting depth. As a result, the process know-how was implemented, providing helpful information for applying different configurations and strategies.

## Materials and Methods

Polyether ether ketone (PEEK), a semicrystalline thermoplastic, is among the world's highest-performing functional materials due to its excellent biocompatibility, chemical resistance, and mechanical and thermal properties, which are retained at high temperatures. This polymer is often used in demanding aerospace, automotive, chemical, and medical applications. A 1.75 mm filament diameter was used. The primary data are reported in Table 1.

The specimens were realized using the FUNMAT HT, a Fused Filament Fabrication (FFF) printer produced by Intamsys Technology Co., Ltd. (Shanghai, China). This printer had a build volume of 260×260×260 mm$^3$. All samples with dimensions 30×60×5 mm$^3$ were printed with a layer height of 300 µm, an infill of 20% with an internal grid pattern, three bottom and three top layers, and five walls (Fig.1). The selected numbers of walls and layers were chosen to sufficiently resist to the grinding loads whereas reducing the final cost of the AM specimens. The printer nozzle was 600 µm diameter. All specimens were printed flat on the build platform (*XY* plane) with a printing speed of 25 mm/s, the nozzle temperature of 410°C, the build plate, and the heating chamber equal to 120°C and 90°C, respectively. For this study, the printing parameters were kept constant after the initial tuning to evaluate the grinding process, not the AM process.

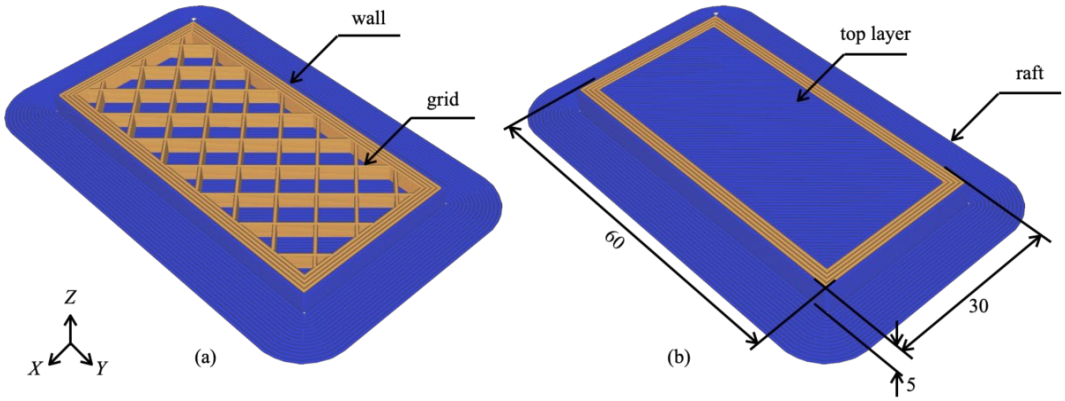


*Fig. 1. Specimen with internal structure (a) and final configuration (b) (all dimensions in mm).*

*Table 1: Material data [8]*

| Physical property | Value | Physical property | Value |
|---|---|---|---|
| Density $\rho$ | 1.30 [g/cm$^3$] | Tensile Strength $\sigma_R$ | 99.9 [MPa] |
| Glass transition temperature $T_g$ | 143 [°C] | Young's modulus $E$ | 3.74 [GPa] |
| Melt temperature $T_m$ | 343 [°C] | Elongation at break | 9.1 [%] |
| Thermal conductivity $\lambda$ | 0.29 [W/m×K] | Impact strength | 7.1 [kJ/m$^2$] |

The specimens were then processed on an instrumented grinding machine, a Planomat 408 CNC machine (Blohm Jung GmbH, Hamburg, Germany), designed and implemented in previous

experiences [9-11]. Based on the Box-Behnken design, a Design of Experiment (DoE) plan was used to conduct, analyze, and interpret controlled tests to evaluate the influence of grinding process parameters on the AM part surface quality. The Box-Behnken design was a very efficient response surface design, giving information on the effect of experiment variables and overall experimental error with a minimum run number [12]. The following characterized it: each factor had three levels, the design focused on fitting a quadratic model with interaction effects, and the ratio of experimental points to the coefficient number was as low as possible. As a response surface design, the design factors (input parameters) were the cutting speed $v_c$, the feed velocity $v_f$, and the depth of cut $a_e$, each with three coded levels (-1, 0, +1) generating 15 runs. The uncoded values are reported in Table 2. The uncoded value ranges were chosen following previous experiments [9-11], focusing on high cutting and feed speed with low depths of cut.

*Table 2: Material data.*

| Design factor | Coded values | Uncoded values |
|---|---|---|
| cutting speed $v_c$ | -1, 0, +1 | 25, 50, 75 [m/s] |
| feed velocity $v_f$ | -1, 0, +1 | 900, 1350, 1800 [mm/min] |
| depth of cut $a_e$ | -1, 0, +1 | 0.10, 0.15, 0.20 [mm] |

The grinding machine used a SINUMERIK 840d sl control (Siemens AG, Munich, Germany) with a Data Acquisition (DAQ) system to register spindle power at a sampling of 0.002 s. The maximum machine spindle limits were 1,450 rpm and 7.5 kW. The wheel was coded as 45A120-5G11RM-LV233/35 (ELBE Schleifmittelwerk GmBh & Co KG, Sachsenheim, Germany) and had an initial diameter of 400 mm and a thickness of 30 mm. Two Slimline cells (Kistler Group AG, Winterthur, Switzerland) were interfaced to measure the normal and tangential forces. A MAXYMOS TYP5877A/B (Kistler Group AG, Winterthur, Switzerland) acquired the cell signals, working as an amplifier and monitoring system, with a sampling of 0.001 s. A type J thermocouple (1.0 mm diameter and 500 mm length), measuring up to 760°C, was also available to measure workpiece temperature. The temperature sensor's tip was 29.5 mm from the pressure plate top, and the hole was filled with epoxy to fix it. The temperature had to be filtered as the power after the data acquisition in the post-processing. All cell signals were acquired, filtered, and post-processed for the following analyses. In particular, the normal $F_n$ and the tangential $F_t$ forces were used as two main response variables of the DoE design. The normal force $F_n$ was usually lower than the tangential force $F_t$. The other response variables were the average roughness $R_a$ and the mean roughness depth $R_z$, determined transversally to the specimen length. The roughness was measured offline using a Conoscan 3000 (Oproprint srl, Rome, Italy), a laser-based conoscopic holographic sensor with a 50 mm lens and an optical resolution of 10 µm. The laser sensor acquisition was performed on a surface patch of $3\times50$ mm$^2$, then extracting the roughness profiles, according to definitions of ISO 21920-2:2021. $R_z$ was almost always greater than $R_a$ because $R_a$ represented the average values, and $R_z$ was based on maximum values. The difference between the two parameters also depended on the roughness profile uniformity. Figure 2 shows the flowchart of the data acquisition system.

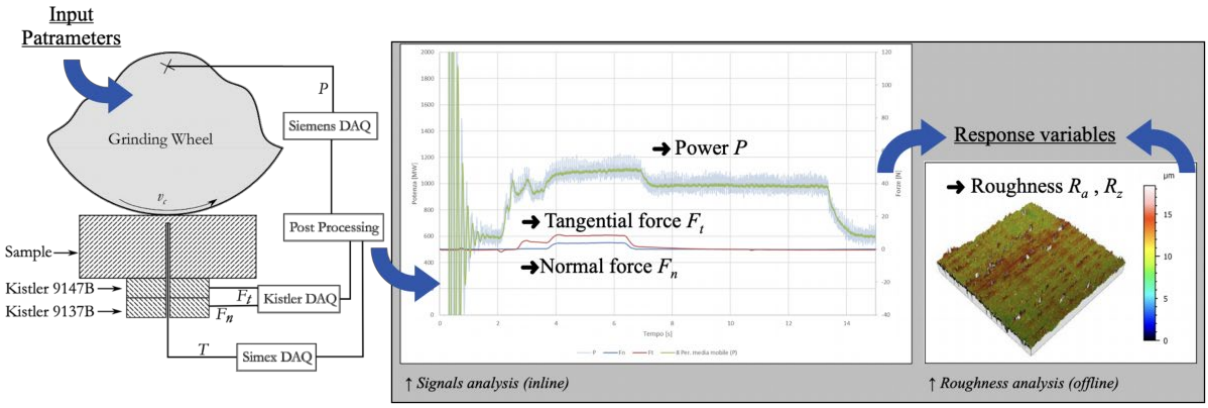


*Fig. 2. Data acquisition flow chart.*

## Results and Discussion

The measures with the thermocouple indicated temperatures below the glass transition in all process conditions. This outcome was associated with a high lubricant flow rate and a low friction coefficient of the PEEK. Reducing temperatures was also crucial to avoid burns on the machined parts and kneading on the grinding wheel [9]. These latter problems were eliminated by adopting a high liquid coolant flow rate and performing an appropriate dressing before use.

The measures of the grinding forces were crucial to evaluate the material machinability. The normal force had a similar trend to the tangential force. Figure 3 presents the experimental results of the Box-Behnken design of the maximum normal $F_n$ and tangential $F_t$ forces. The experiment number identified the triplet of the process parameters $v_c$, $v_f$, and $a_e$ in the side table.

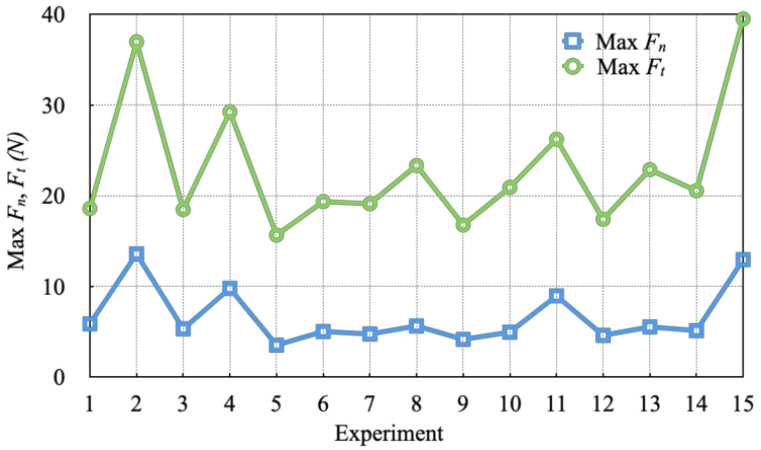


| Experiment | $v_c$ (m/s) | $v_f$ (mm/min) | $a_e$ (mm) |
|---|---|---|---|
| 1 | 75 | 1800 | 0.15 |
| 2 | 25 | 1800 | 0.15 |
| 3 | 50 | 1350 | 0.15 |
| 4 | 25 | 900 | 0.15 |
| 5 | 50 | 900 | 0.1 |
| 6 | 75 | 900 | 0.15 |
| 7 | 50 | 1350 | 0.15 |
| 8 | 75 | 1350 | 0.2 |
| 9 | 75 | 1350 | 0.1 |
| 10 | 50 | 1350 | 0.15 |
| 11 | 25 | 1350 | 0.1 |
| 12 | 50 | 1800 | 0.1 |
| 13 | 50 | 1800 | 0.2 |
| 14 | 50 | 900 | 0.2 |
| 15 | 25 | 1350 | 0.2 |

*Fig. 3. Experimental data results of the maximum $F_n$ and $F_t$.*

The Analysis of Variance (ANOVA) was employed to estimate the impact of the grinding process parameters and their interactions on the selected response variables, computing suitable regression models. From the first data analysis, both forces were reduced with a decrease of the cutting depth $a_e$ and an increase of the cutting speed $v_c$. The feed speed $v_f$ had a slight effect on force variations. Response surfaces of the maximum measured normal force $F_n$ (Figure 4) and tangential force $F_t$ (Figure 5) corroborated the above analysis. The coefficient of determination $R^2$ of both responses was greater than 97%, confirming the excellent prediction of the statistical model.

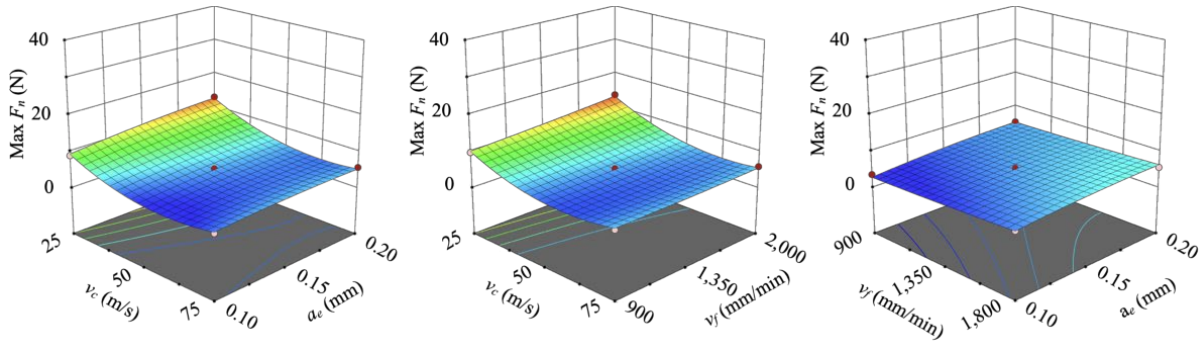


*Fig. 4. Maximum normal force $F_n$ graphs.*

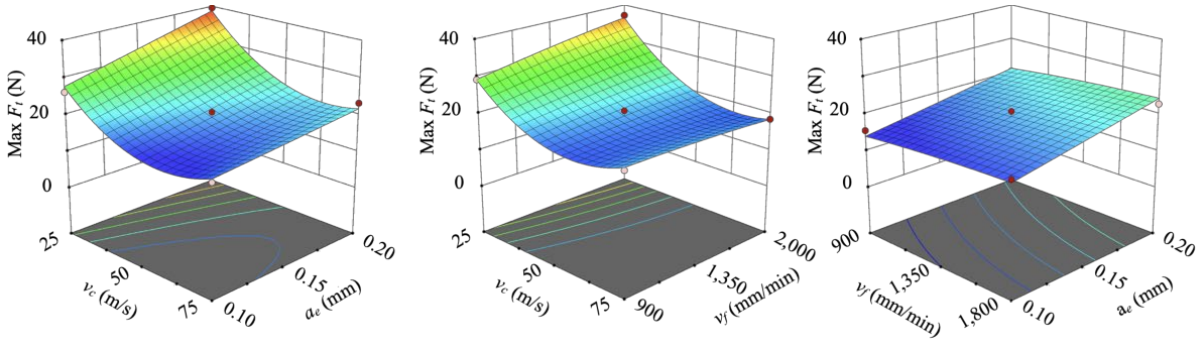


*Fig. 5. Maximum tangential force $F_t$ graphs.*

The lowest values of the normal and tangential forces were achieved for high $v_c$ and low $v_f$ and $a_e$. Low force values reduced wheel abrasive shedding, pore blockage, and machined surface damages. These results were coherent with the analysis of the maximum cutting depth $h_{max}$, correlated to the process parameters with the following equation:

$$h_{max} = \sqrt{\frac{6}{C \times r} \times \frac{v_f}{v_c} \times \sqrt{\frac{a_e}{d_e}}} \tag{1}$$

where $C$ is the number of cutting points per unit area, $r$ is the average effective chip width to undeformed chip thickness ratio, and $d_e$ is the equivalent wheel diameter. $h_{max}$ increased with an increase of $a_e$ and $v_f$, and decreased with $v_c$ increase. The greater the value of $h_{max}$ was, the larger the volume of material removed and the greater the grinding force was.

The measures of the surface roughness allowed the assessment of the surface quality of the final components. Figure 6 presents the experimental results of the Box-Behnken design in terms of the average roughness $R_a$ and the mean roughness depth $R_z$. The experiment number identified the triplet of the process parameters $v_c$, $v_f$, and $a_e$ in the side table. The roughness values were one order lower than the rough components. The ANOVA results showed that $R_a$ increased with low $v_c$, $a_e$, and high $v_f$. The same trend was also evident for $R_z$. The surface roughness was closely related to the maximum cutting depth [13], as reported from the following relation:

$$R_t \propto \sqrt[3]{\frac{{h_{max}}^4}{a_e}} \approx \sqrt[3]{\left(\frac{v_f}{v_c} \times \frac{1}{C \times r \times \sqrt{d_e}}\right)^2} \tag{2}$$

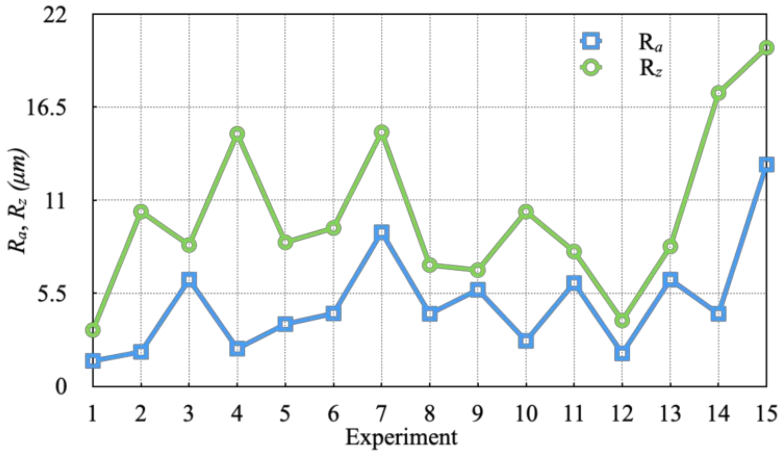


| Experiment | $v_c$ (m/s) | $v_f$ (mm/min) | $a_e$ (mm) |
|---|---|---|---|
| 1 | 75 | 1800 | 0.15 |
| 2 | 25 | 1800 | 0.15 |
| 3 | 50 | 1350 | 0.15 |
| 4 | 25 | 900 | 0.15 |
| 5 | 50 | 900 | 0.1 |
| 6 | 75 | 900 | 0.15 |
| 7 | 50 | 1350 | 0.15 |
| 8 | 75 | 1350 | 0.2 |
| 9 | 75 | 1350 | 0.1 |
| 10 | 50 | 1350 | 0.15 |
| 11 | 25 | 1350 | 0.1 |
| 12 | 50 | 1800 | 0.1 |
| 13 | 50 | 1800 | 0.2 |
| 14 | 50 | 900 | 0.2 |
| 15 | 25 | 1350 | 0.2 |

*Fig. 6. Experimental data results of $R_a$ and $R_z$.*

where $R_t$ was the total height of the roughness profile. $R_z$ was computed by averaging successive values of $R_t$ calculated over the evaluation length. The most influencing factors on $R_a$ and $R_z$ variations were $a_e$ and $v_c$. Increasing the $a_e$ while reducing $v_c$ produced a greater chip thickness and higher $R_a$ and $R_z$. The interactions between $a_e$ and $v_c$ resulted in increased force, causing more wheel vibration and increased surface roughness. Response surfaces of the transversal average roughness $R_a$ (Figure 7) and the transversal mean roughness depth $R_z$ (Figure 8) supported the above analysis. The coefficient of determination $R^2$ of both responses was greater than 93%, confirming the excellent prediction of the statistical model.

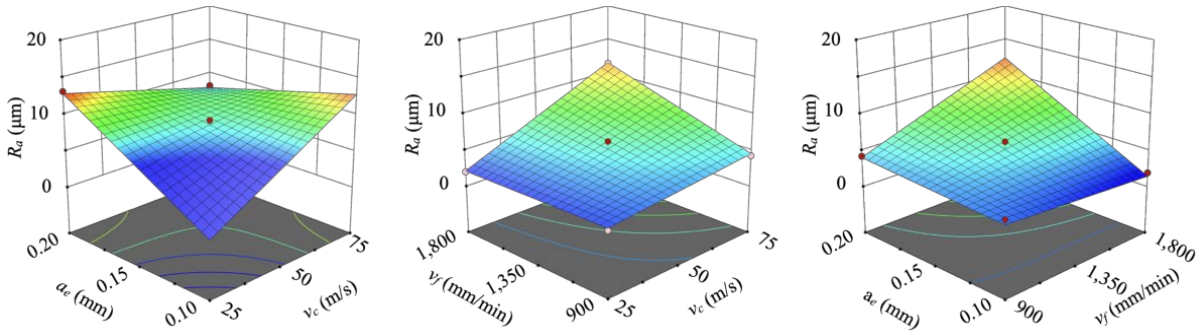


Fig. 7. Average roughness $R_a$ graphs.

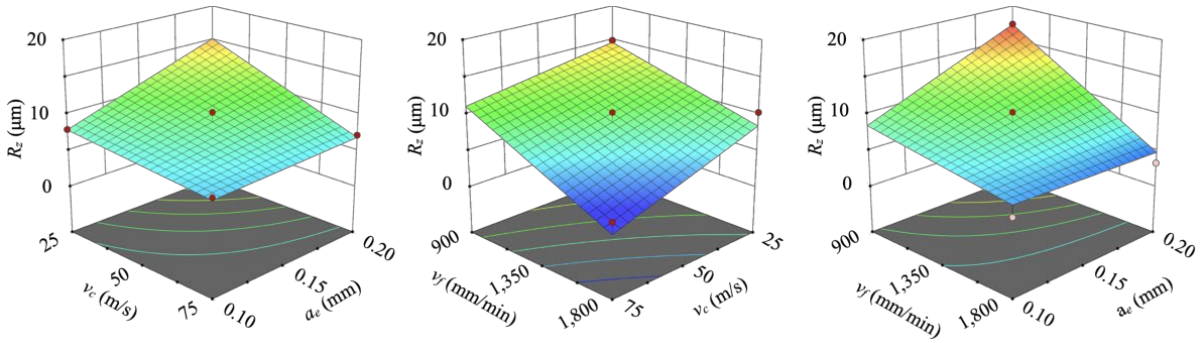


*Fig. 8. Mean roughness depth $R_z$ graphs.*

## Conclusions

This work investigated the performance of additively manufactured PEEK regarding grinding forces and surface roughness. In particular, PEEK specimens were examined using several process parameters according to the Design of the Experiment plan. The grinding forces were monitored in real time while profile roughness was computed offline.

The following conclusions can be drawn from the experimental results. The grinding forces were positively correlated with the depth of cut $a_e$ and feed speed $v_f$, and negatively associated with the cut speed $v_c$. The lowest values of the normal $F_n$ and tangential $F_t$ forces were achieved for high $v_c$ and low $v_f$ and $a_e$. The surface quality of the ground parts was significantly better than the rough parts, approximately one order of magnitude lower. The most influencing factors on the average roughness $R_a$ and the mean roughness depth $R_z$ were the depth of cut $a_e$ and the cut speed $v_c$. The surface quality was effectively improved by reducing the depth $a_e$ and the feed speed $v_f$, increasing the cut speed $v_c$.

## Acknowledgments

The authors thank Prof Luigi Galantucci and Prof Fulvio Lavecchia of Politecnico di Bari for their suggestions, Marco Massari and Giuseppe Glionna of Tecnologie Diesel S.p.A for the experimental support.

The Project was funded under the program Department of Excellence - Law number 232/2016 (Grant No. CUP - D93C23000100001), the National Recovery and Resilience Plan (NRRP), Mission 4 Component 2 Investment 1.3 - Call for tender No. 341 of 15/03/2022 of the Italian Ministry of University and Research (MUR), funded by the European Union – NextGenerationEU, and the RIPARTI funding (assegni di Ricerca per ripartire con le Imprese) of the Apulia Region.

## References

[1] Y. Chen et al. Study the dynamic influence of the distribution of cutting depth on the ground surface quality in a precision grinding process. Journal of Manufacturing Processes 107 (2023) 134-143. https://doi.org/10.1016/j.jmapro.2023.10.028

[2] K.Kanishka, B. Acherjee. A systematic review of additive manufacturing-based remanufacturing techniques for component repair and restoration. Journal of Manufacturing Processes 89 (2023) 220-283. https://doi.org/ 10.1016/j.jmapro.2023.01.034

[3] A. Beaucamp, B. Kirsch, W. Zhu. Advances in grinding tools and abrasives. CIRP Annals - Manufacturing Technology 71 (2022) 623646. https://doi.org/ 10.1016/j.cirp.2022.05.003

[4] D. Aslan, E. Budak. Surface roughness and thermo-mechanical force modeling for grinding operations with regular and circumferentially grooved wheels. Journal of Materials Processing Technology 223 (2015) 75-90. https://doi.org/10.1016/j.jmatprotec.2015.03.023

[5] A. Bell, T. Jin, D.J. Stephenson. Burn threshold prediction for High Efficiency Deep Grinding. International Journal of Machine Tools & Manufacture 51 (2011) 433-438. https://doi.org/10.1016/j.ijmachtools.2011.01.006

[6] P. Wang, B. Zou, S. Ding. Modeling of surface roughness based on heat transfer considering diffusion among deposition filaments for FDM 3D printing heat-resistant resin. Applied Thermal Engineering 161 (2019) 114064. https://doi.org/10.1016/j.applthermaleng.2019.114064

[7] A. Pulipaka et al. Effect of 3D printing process parameters on surface and mechanical properties of FFF-printed PEEK. Journal of Manufacturing Processes 85 (2023) 368-386. https://doi.org/10.1016/j.jmapro.2022.11.057

[8] Information on https://www.intamsys.com/

[9] R. Spina, B. Cavalcante. Evaluation of grinding of unfilled and glass fiber reinforced polyamide 6,6. Polymers, 12 (2020) 1-11. https://doi.org/10.3390/polym12102288

[10] R. Spina et al. Forces and specific energy of polyamide grinding. Materials, 14 (2021) 5041. https://doi.org/10.3390/ma14175041

[11] R. Spina et al. Analysis of surface grinding of thermoplastics specimens with inline measurements. Journal of Manufacturing and Materials Processing, 6 (2022) 81. https://doi.org/10.3390/jmmp6040081

[12] NIST/SEMATECH e-Handbook of Statistical Methods. Information on https://www.itl.nist.gov/div898/handbook/pri/section3/pri3362.htm.

[13] I.D. Marinescu et al. Handbook of machining with grinding wheels. CRC Press. https://doi.org/10.1201/b19462